HHS Public Access

Author manuscript

Annu Rev Anal Chem (Palo Alto Calif). Author manuscript; available in PMC 2018 February 19.

Published in final edited form as:

Annu Rev Anal Chem (Palo Alto Calif). 2016 June 12; 9(1): 1–25. doi:10.1146/annurev-anchem-071015-041742

Applications of Optical Microcavity Resonators in Analytical Chemistry

James H. Wade and **Ryan C. Bailey**

Department of Chemistry, University of Illinois at Urbana-Champaign, 600 S. Mathews Ave., Urbana, IL, 61801

Abstract

Optical resonator sensors are an emerging class of analytical technologies that use recirculating light confined within a microcavity to sensitively measure the surrounding environment. Bolstered by advances in microfabrication, these devices can be configured for a wide variety of chemical or biomolecular sensing applications. The review begins with a brief description of optical resonator sensor operation followed by discussions regarding sensor design, including different geometries, choices of material systems, methods of sensor interrogation, and new approaches to sensor operation. Throughout, key recent developments are highlighted, including advancements in biosensing and other applications of optical sensors. Alternative sensing mechanisms and hybrid sensing devices are then discussed in terms of their potential for more sensitive and rapid analyses. Brief concluding statements offer our perspective on the future of optical microcavity sensors and their promise as versatile detection elements within analytical chemistry.

Keywords

whispering gallery mode; biosensing; chemical sensing

1. Introduction

Advances in micro- and nanofabrication methods have played key roles in advancing analytical measurement technologies. Many of these capabilities have their genesis in the microelectronics industry, which has followed Moore's Law towards continuously miniaturized complementary metal oxide semiconductor (CMOS) transistors (1). A byproduct of improved CMOS processing is the reliable and scalable fabrication of micro- and nanoscale sensing devices (2). Though the principal focus of the microelectronics industry has been the manipulation of electrons on microchip devices, light can also be manipulated on slightly longer scales by the fabrication of photonic structures such as waveguides and other resonant microcavities (3). These photonic circuits are most typically fabricated from semiconducting materials and often operate at standard telecommunication wavelengths (4–6). Such devices have many applications beyond the realm of traditional optical sensing, including optical interconnects, signal routing and processing, and long range telecommunications (7–10). Leveraging the ability to precisely and sensitively manipulate light on such small scales, optical resonators are playing an increasingly important role in analytical chemistry, finding applications to a multitude of analyte classes (11–14). While impressive results have been reported, the promise of optical resonators will

only be realized through the translation of devices beyond proof-of-concept demonstrations and their application to real-world molecular detection challenges, ranging from on-site environmental monitoring to personalized medicine.

Microcavity sensors share the common property that they confine light into a circular path and enhance the local electromagnetic field through a constructive interference resonance condition. Owing to similarities in interference-based modes that can satisfy propagating resonance conditions, these sensors are commonly called whispering gallery mode (WGM) resonators, referring to the acoustic phenomenon first described by Lord Rayleigh at the beginning of the 20th century (15). In microcavity resonators, light couples into the microcavity only at specific wavelengths, λ_r, under conditions of optical resonance, as defined by:

$$\lambda_r = \frac{Ln_{eff}}{m}$$

where L is the circumference of the cavity, n_{eff} is the effective refractive index sampled by the optical mode, and m is an integer representing the azimuthal quantum number. Changes in the effective refractive index at the sensor surface result in shifts in resonant wavelength coupled into the cavity. Light coupled into the resonant cavity results in a drop in the intensity of the light transmitted through the linear coupling waveguide as it propagates past the sensor and measurements are most commonly reported as changes in relative shift of the resonance wavelength ($\Delta\lambda_r$) (Figure 1).

A defining factor used to compare optical microcavities is the quality (Q) factor, defined as the ratio of the resonant wavelength λ_r to the spectral linewidth of the resonance ($\delta\lambda$):

$$Q = \frac{\lambda_r}{\delta\lambda}$$

The Q-factor is related to the photon lifetime within the cavity and is proportional to the number of times the light circulates within the microcavity. The high sensitivity of optical resonators derives from the repeated sampling of analytes near the sensor surface as light continuously propagates around the optical microcavity, drastically increasing the effective path length. Q-factors ranging from 10^3 to 10^{10} have been reported in the literature (16, 17), correlating to effective path lengths in excess of a centimeter.

More than a decade has passed since the first demonstrations of sensing with optical resonators (3, 18–20); however, their rapid growth in recent years is the culmination of advances in new sensor designs, increasing speeds of signal readout, and low-cost microfabrication, as well as key developments in supporting technologies (e.g., lasers, photodetectors, precision optics, microfluidics). The end result is a group of technologies that is beginning to make substantive impacts throughout analytical chemistry and related fields.

Given the existing literature available for optical resonator sensors, there are a number of excellent reviews already available, and we point the reader to other resources with more comprehensive coverage of topics only briefly mentioned in this review (12–14, 21–29). This review seeks to highlight key developments in optical resonator sensing with a focus on the practical implementation of these devices to solve challenging analytical problems. First, we survey recent technological improvements in device fabrication, as well as discussing the major criterion in designing an optical resonator. We then survey notable applications of optical resonators as sensors, such as biomolecule and gas detection. We follow the discussion of applications by addressing the practical limits of optical resonators with an eye towards what is likely to come in the near future. Included in this discussion is the emergence of hybrid sensors that seek to combine the benefits of optical sensors with that of other existing measurement technologies, ranging from plasmonic materials to optomechanical devices and on-chip lasing.

2. Design of Optical Resonator Sensors

Optical resonator sensor design often involves a compromise between improved sensor sensitivity and scalable sensor fabrication. Rigorous micro- and nanofabrication methods, precise manipulation of high performance optical components, and advanced data processing methods enable sensors to push toward high Q-factors and more robust performance. Conversely, many of these improvements to an individual sensor's performance come at the cost of scalable manufacturing and facile sensor operation within practical analytical environments (e.g., benchtop, point-of-care, field analysis).

2.1 Device Geometry

The common feature of WGM sensors is a circular path that defined an optical microcavity through which light is confined. Many early resonator geometries were simple structures such as spheres (16, 20, 30–33), toroids (17, 34), discs (19, 35–37), and rings (38–40). More recently, geometries including tubes (41–43), capillaries (44–48), bubbles (49), and knots (50) have also found utility. Figure 2 provides an overview of established sensor geometries.

An ideal microcavity that perfectly confined light would have an infinite Q-factor. However, perfect cavities cannot be experimentally realized as small geometric imperfections or absorptive losses prohibit perpetual confinement. Higher Q-factors are due to stronger confinement of photons within the waveguide material, which is in turn is proportional to the mode volume (V). Sensor design often seeks to maximize the Q/V ratio by fabricating smaller resonant structures, but optical losses from higher bending radii reduce the Q-factor (51). Sensor development has now focused on improved sensor geometries with a bending radius >5 μm with improved fabrication practices to maximize Q-factor.

In order to achieve high Q-factors, microcavities must be fabricated with low surface roughness, thereby reducing waveguide scattering losses (17). Microtoroid fabrication includes a reflow smoothing process to limit scattering losses, but common reflow techniques are limited to small sensor sizes (<500 μm) and the sensor geometry itself is not easily integrated within a conventional semiconductor fabrication workflow (52, 53). To limit scattering losses, Lee et al (52) have utilized wedge-shaped waveguides. Since

propagating modes in a wedge geometry are pushed away from scattering surfaces, fabrication defects have a reduced effect on Q. This approach is also compatible with conventional semiconductor processing.

Goblet and conical geometries offer Q-factors ranging from 10^5 to 10^7 by processing a polymer layer directly on top of a silicon substrate (54–56). These devices cannot match the Q-factor of toroidal or wedge geometries, though they offer potential lower-cost fabrication that can be parallelized. Specifically, the goblet geometry is formed from the surface tension induced by a thermal reflow step. The polymeric material has reduced surface roughness compared to standard lithographic methods, and the material is compatible with replica molding, though this requires a mold from an ultra-high Q-factor device (55).

2.2 Sensor Interrogation

The ability to fabricate optical microcavities reproducibly with Q-factors $>10^5$ has now become routine. Therefore practical applications of these technologies now are intimately tied to the ability to reproducibly couple light into these ultra-high Q optical microcavities. An ideal coupling strategy for many downstream applications would be free from complex optical setups (e.g., floated laser table) and capable of operating under ambient conditions. The first generation of microsphere resonators coupled light into the microsphere by aligning an adiabatic fiber taper so that the fiber overlapped with the evanescent field of the microsphere (20, 57). While this method allows for efficient coupling into the resonator geometry, optical alignment can be tedious and complicates operation of these devices outside of a well-controlled laboratory setting. Additionally, multiplex measurements are difficult to achieve with this arrangement due to rigorous demands of optical alignment and the challenge of simultaneously or serially interrogating multiple microcavity sensors. Alternatively, some geometries are well-suited to coupling via chip-integrated planar waveguides, obviating the need for fiber extrusion and alignment (20, 58–61). For integrated waveguides, light is coupled onto the chip by fiber-optic to waveguide coupling, edge coupling from the tunable light source to the waveguide, or surface couplers (e.g., grating couplers) (51). Fiber-optic to waveguide coupling and edge coupling require precise optical alignment of either an optical fiber or laser with the waveguide, which poses similar limits as fiber taper coupling methods. Surface couplers have greater tolerances for optical alignment because the size of the surface couplers can be larger than the waveguide (62, 63). A disadvantage of free space coupling with grating couplers is that often only a fixed polarity of light can be used (24).

There are additional possibilities for coupling light into microspheres. For example, microspheres resting on a surface can be interrogated via a prims (32, 64, 65). Additionally, the use of fluorescent microparticles as the microcavity itself eliminates the need for optical waveguides or fiber-optics altogether, as the fluorescence generated by a focused laser spot can be confined within the microcavity (66–68). The approach has been termed whispering gallery mode imaging, and multiplexing can be achieved by using particles of difference sizes and fluorescent wavelengths. Mass transfer advantages also come into play with microparticles as analyte capture can be achieved in free solution prior to interrogation

bound to a planar substrate (64). Figure 3 illustrates several common methods of optical microcavity interrogation.

2.3 Sensor Materials

Beyond considerations in terms of ease of fabrication, the choice of material for optical resonator design is also guided by the ability of the resulting cavity to strongly confine light. The higher the refractive index contrast between the cavity and the surrounding material, the greater the optical confinement. The length evanescent field extending into the sensing region is inversely proportional to the strength of confinement. Lower index contrast between cavity and sensing region leads to a larger percentage of the evanescent field extending into the sensing region, which then samples the local environment. Evanescent field strength (I) decays exponentially from the sensor surface as described by:

$$I(z)=I_0e^{2\gamma z}$$

where I_0 is in the initial field strength at the sensor surface, z is the distance from sensor surface, and γ is an exponential decay constant that describes the rate of field fall off (30, 69). Taken together, the choice of materials system effects not only the degree of optical confinement (Q-factor), but also the proportion of light that can interact with the sensing region. Therefore materials system selection should be considered as one balances Q-factor against evanescent field penetration depth, which may vary depending upon the ultimate application of the device.

Due to their general ease of fabrication, silicon-based materials systems have been well-developed for microresonator sensing applications (13). In addition to silicon-on-insulator (SOI), materials such as silicon carbide (SiC) and silicon nitride (Si_2N_3) have been used for sensor fabrication due to their impressive near-infrared zero-phonon emission and strong refractive index contrast with SiO_2, respectively (70, 71). Hydrogenated amorphous silicon (a-Si:H) has also been used due its high refractive index (~3.5), low loss compared to crystalline SOI, and versatility in fabrication, as it can be deposited at lower temperatures(≤ 300°C) (72). Titanium oxide (TiO_2) is a useful material for WGM sensors due to low absorption in the visible and infrared wavelengths, a low thermal expansion coefficient, a negative thermo-optic coefficient, biocompatibility, and compatibility with CMOS microfabrication (73). Barium-titanate ($BaTiO_3$) microspheres have also been used for sensing, offering non-optical advantages in terms of being able to perform measurements in small volumes (10 μL), commercial availability, and facile surface functionalization methods (64, 65).

Various organic polymer materials have been used for optical microcavity fabrication (54, 55, 67, 74–85). The principal advantage of these materials is low-cost, simple manufacturing, and many of the resulting devices, such as the polymer microgoblets, maintain remarkable optical qualities with Q-factors as high as 10^6 (54). Polymers doped with fluorescent dyes and quantum dots have also been used to coat the inner walls of optofluidic resonators (46, 47). Isolated conjugated polymers (ICPs) are a particularly interesting material for WGM sensing, as they possess the advantages of free-space coupling

(discussed above), inherent fluorescence (i.e., no doping needed), and simple synthesis/fabrication methods (67). However, additional developments are needed to realize full functionality as optical resonator sensors. Specifically, at present ICPs have a Q-factor of only 600 and a low refractive index (1.6–1.8), which would make sensing in liquid environments challenging.

2.4 Sensing Mechanisms

Nearly all implementations of optical resonators incorporate some form of photodetector monitoring intensity over time. As discussed above, high Q-factor devices will support spectrally narrow resonances that will shift as the local refractive index is modulated (**Eq. 1**). That is to say that as Δn_{eff} changes at or near the sensor surface, spectral shifts in the positions of resonances can be monitored as a function of time. Often presented as a drop in intensity measured by a photodetector of light propagating through the linear waveguide past the microcavity, these resonances have a Lorentzian line shape that follows:

$$I(\lambda)=I_0-\beta\left(\frac{(\delta\lambda/2)^2}{(\lambda-\lambda_r)^2+(\delta\lambda/2)^2}\right)$$

where $I(\lambda)$ is the photodetector current as a function of wavelength, I_0 is the is the measured current under non-resonant conditions (100% transmission—maximum current) and β is the coupling efficiency. Importantly, sensing results can be reported in terms of a relative wavelength shift, $\Delta\lambda_r$, as opposed to an absolute wavelength value.

One limiting factor in the ability to precisely determine shifts in resonance wavelength is the tuning precision of the tunable lasers used to interrogate microcavities. Wavelength uncertainties as high as 20 pm can be encountered due to frequency jitter and non-ideal scan-voltage control. One method to improve the noise floor while still using a tunable laser is to scan a large spectral window (>12 nm) through multiple free spectral ranges (FSRs) in order to track multiple λ_r within a single transmission spectrum. This method can reduce the noise for optical resonators with moderate Q-factors (10^4) from >10 pm to as little as 0.1 pm, corresponding to a limit of detection (LOD) on the order of 10^{-7} refractive index units (RIUs) (58). While higher Q-factors would assist in lowering the noise floor even further, Lu et al (86) achieved significant improvements in the noise floor by incorporating a thermally-stabilized interferometer and successfully resolved a 0.1 fm shift above background. Aside from laser-induced noise contributions, thermal fluctuations are a major contributor to noise. To circumvent thermal noise, controls can be integrated onto a sensor array by coating some of the sensors within an inert polymer (58, 87). The coated sensors should readily respond to thermal changes but are shielded from bulk RI changes or surface binding events.

As an alternative to measuring shifts in resonance wavelengths, resonance broadening and mode splitting can also be monitored for sensing applications. Linewidth broadening refers to the increase in $\delta\lambda$, which represents a loss in Q-factor. This type of sensing is particularly useful for monitoring nanoparticle binding, which causes a loss of Q due to absorption and scattering losses (88, 89). Mode splitting occurs do to scatter-induced coupling between degenerate, counter-propagating spectral modes and results in the splitting of a single

resonance peak into two resonances. This is most commonly observed when a relatively large object, such as a nanoparticle, enters the evanescent field and splits a single resonance mode into two via scatter-induced coupling (90). A significant benefit of a mode splitting-based detection experiment is that noise from thermal fluctuations is effectively canceled out, as the susceptibilities of degenerate propagating modes are identical, and while the absolute wavelength of resonances might shift, the degree of spectral splitting is temperature insensitive. These methods have been employed primarily in simultaneous detection and sizing of nanoparticles (90–92); however, this approach is limited to applications in which the target(s) being detected have substantial enough scattering properties to generate a split resonance. Monitoring the intensity of back-scattered light from the resonator instead of transmittance can be used to improve the noise floor of WGM sensing below what can be achieved with monitoring of mode splitting alone. Proof-of-concept experiments using an AFM tip to simulate the presence of a biomolecule on a microtoroid resonator surface demonstrated a reduction of frequency noise by seven dB and a noise floor of 76 kHz (93).

Another interesting measurement approach that demonstrated utility of microcavity resonators beyond simply measuring the presence or amount of bound target involved the simultaneous interrogation with transverse magnetic (TM) and transverse electric (TE) propagating modes. When the resonator material is birefringent (i.e., refractive index of the material is dependent on polarization of the light), each mode will have a distinct resonance response, which in turn can be used to extract biomolecular orientation on the sensor surface (94).

3. Applications of Optical Resonators

The simplest implementation of an optical resonator sensor is for bulk refractive index sensing using an unmodified sensor surface (46, 47, 95, 96). Unmodified sensors can also be used to monitor adsorption and/or desorption of an analyte onto the sensor surface, such as bovine serum albumin (BSA) (20, 30, 55, 57). That said, the greatest value of optical resonators in analytical chemistry lies in leveraging the exquisite surface sensitivity of the devices when functionalized with target-specific capture agents. Capture agents having high binding affinities and target specificities can be bound to the sensor surface—many times using standard covalent coupling reactions with chemically-modified sensors. Without question, the most extensively explored application of microcavity resonators has been for biosensing applications, and that will be the focus of the following sections. However, other applications to gas sensing, liquid chromatographic eluent detection, and heavy metal detection are also discussed. Other intriguing measurement modes that take advantage of unique electromagnetic field, force, pressure, and temperature effects of microcavity resonators are beyond the scope of this review; however, interested readers are referred elsewhere (12).

3.1 Biosensing

The biosensor community has placed a large emphasis on the development of label-free detection strategies. Herein, we use the phrase “label-free” to broadly describe detection without chemical modification to the analyte molecule. However, this does require that the

sensor surface be modified with a target-specific capture agent (e.g., DNA, antibody). This is often achieved by derivatizing the surface with a reactive functional group and then using standard bioconjugation techniques (97), though other methods have been utilized (26, 97).

Importantly, the performance characteristics of the resulting sensors are almost always extremely dependent on the binding properties of the capture agent (affinity and specificity), as well as the matrix in which the detection was performed. Therefore, one must take caution when singularly comparing limits of detection from the literature to define the relative promise of a particular device. That is to say that for an identical device, the limit of detection for a biotin-streptavidin interaction (K_D ~ 1 fM) should be 4-orders of magnitude lower than for even a very good antibody-antigen binding pair (K_D ~ 10 pM) simply on the basis of binding affinity along—having absolutely nothing to do with sensor performance. This word of caution is provided as readers should be careful when interpreting the relative performance of different devices as applied to different targets and from within different complexities of sample matrix. One other caution for readers in this field is to be sure to appreciate the difference between moles and molar (moles/L) concentrations. These two units are commonly used in reporting limits of detection, though their significance is highly dependent upon the sampled volume. Specifically, the absolute number of molecules in a solution may be very small for a small volume analysis even though the relative concentration, which relates directly to the number of proportionally-bound analyte molecules through the equilibrium dissociation constant K_D, is equivalent to other reports that simply detected from a larger volume.

As eluded to above, an extremely simplistic biomolecular binding system is biotin-avidin binding (39, 40). The assay can work by tethering either biotin or an avidin derivative (e.g., streptavidin, neutravidin, etc.) to the sensor surface and monitoring binding of the corresponding target to the sensor surface. The biotin-avidin interaction is the strongest known non-covalent binding interaction (98). Therefore, this biotin-avidin pair can almost effectively be considered as a covalent bond, and this binding affinity does not adequately represent typical receptor-target interactions. As a result, concentration-based LODs determined using this system are not correlative of real-world biosensing performance. Sensor validation efforts focusing on more realistic targets and more complex matrices should be viewed as more relevant within the biosensing community.

Nucleic acid detection relies on immobilization of capture strands of DNA onto the sensor surface (99, 100). Nucleic acids have strong selectivity for binding to specific complementary sequences, as dictated by Watson-Crick base pairing interactions. Using microcavity sensors, single nucleotide mismatch discrimination is often achievable under appropriate experimental conditions (99–101). Recently, Shin et al (102) used silicon microring resonators to detect single nucleotide polymorphisms (SNPs) of two commonly mutated genes in bladder cancer, FGFR3 and HRAS, in spiked urine samples. In cases where label free detection of nucleic acids does not provide sufficient signal output, amplification strategies, such as polymerase chain reaction (PCR) can be used. Sabaté del Río et al (103) designed an on-chip solid-phase recombinase polymerase amplification method capable of real time amplification of a DNA target with a LOD of 780 fM in buffer conditions. In an attempt to avoid the need for PCR-based or other amplification methods,

Wu et al (104) implemented a DNA strand displacement circuit for detection using a WGM sphere with an LOD of 32 fmol. Binding of the target sequence to its complement triggers a catalytic network amplification, where the binding of a single target molecule triggers the release of multiple sequences form a multi-stranded precursor complex. This represents a 25-fold improvement over previous microcavity-based methods for DNA detection without PCR-based amplification. Detection of methylation patterns in DNA sequences also promises to provide insight into the epigenetic regulation of gene transcription, ultimately controlling cell and organismal phenotype (105). Hawk and Armani (106) reported a microtoroid cavity modified with methylation-specific antibodies and used it to detect methylated DNA in buffer without the need for PCR amplification or fluorescent tagging.

The aforementioned previous reports of nucleic acid detection serve as valuable proof-of-concept demonstrations; however, further validation in the context of real biological systems have also been pursued using microcavity resonators. In a follow up to their earlier study, Shin et al (107) developed a novel signal amplification to detect mutant genes from non-small cell lung cancer (NSCLC) cells. The method used isothermal solid-phase amplification/detection (ISAD) and a double mismatched primer (DMP) set to improve specificity. The assay took only 20 min to complete and successfully recognized mutant EGFR genes in a mixture of 1% mutant and 99% wild type cells. For the detection of longer sequences, secondary structures can introduce steric interference with capture agent binding. Consequently, most assay designs for nucleic acid detection have focused on shorter (<150 bp) sequences. Kindt et al (108) used short sequences of DNA as chaperones to enable the detection or whole mRNA transcripts in isolated total RNA from HL-60 cells. The chaperones bound to flanking regions surrounding the target binding sequence of the mRNA transcript. By binding to these flanking regions, the secondary structure of the mRNA was disrupted, enabling the mRNA to bind to the capture region on the sensor surface. A bead-based signal enhancement was then used to enable a LOD of 512 amol. Figure 4 provides an overview of the nucleic acid detection and amplification methods discussed above.

As an alternative to signal or analyte amplification methods for nucleic acid detection, decreasing the noise floor allows for detection of oligonucleotides reaching the single molecule limit. Unlike detection of other biomolecules, such as proteins and metabolites, commonly implemented nucleic acid isolation methods result in samples with similar off-target binding as seen in buffer conditions (109, 110). These samples are sufficiently processed such that biological noise may no longer be the dominant contributor to the uncertainty of the measurement. Baaske et al (111) fabricated a WGM sensor capable of monitoring single molecule interactions of nucleic acids as small as eight nucleotides. The sensor is a glass microsphere with a gold nanoparticle attached to the sensor surface. The nanoparticle greatly enhances the optical field strength enabling the discrimination of single-molecule binding events (Figure 5). To ensure that specific binding events only occurred on the nanoparticle surface, only the nanoparticle was functionalized with thiol-modified capture oligonucleotides. The ability to monitor single molecule binding events obviates the need for signal or target amplification methods, while also opening up possibilities for stochastic sensing (112). While the detection of an 8-mer DNA strand is an impressive analytical feet, it should be noted that practical implementation of such a sensor would likely utilize longer sequences that encode greater biological significance.

Proteins are also a routinely targeted class of biomolecules for biosensor development. Common capture agents utilized in microcavity-based protein detection include antibodies (60, 77, 113) and aptamers (114, 115). The limiting step in development of protein detection assays for new protein targets is often validation of high affinity and specific capture probes. The lack of formulaic antibody generation methods (i.e. not simply sequence complementarity as in nucleic acid detection) is a significant barrier faced by all antibody-based detection schemes, as is antibody cross-reactivity, which limits the potential for multiplexing. Antibodies also suffer from narrower working conditions (e.g., pH range, buffer composition) and a tendency to denature and degrade more quickly than nucleic acids. Aptamers are another alternative that hold potential to avoid many of the drawbacks of antibodies, but generation of high affinity aptamers for a wide range of protein targets has proven challenging. In recent years, alternative capture agents have been used for biomolecule detection such as phage proteins (116) and genetically modified virus-like particles (117), which could offer improvements in stability and even self-assembly. As an alternative to standard immunoglobulin antibodies, single domain antibodies have enhanced stability and resistance to denaturation, and Shia and Bailey (118) previously incorporated these capture agents into a microcavity-based detection platform.

Many recent developments in protein detection using microcavity resonators have focused on performing multiplexed measurements while improving signal enhancement methods to measure ultra-low analyte concentrations and to perform measurements in complex matrices (e.g., serum). De Vos et al (77) demonstrated multiplexed detection of antibodies using microring resonators capturing parallel readout of all sensors using an infrared camera reporting a mass sensitivity of 3.4 pg/mm^2. Dunn and coworkers (66, 68) applied WGM imaging detection of established biomarkers, including tumor necrosis factor α (TNF-α), cancer antigen 125 (CA-125), and osteopontin. Using $BaTiO_3$ microspheres of varying sizes, they performed multiplexed measurements from serum samples of these cancer biomarkers with a detection limit below 100 pg/mL, an improvement upon enzyme-linked immunosorbent assays (ELISA). In an impressive display of sensor detection limits, Dantham et al (119) demonstrated the label-free detection of a single protein molecules, including thyroglobulin (Tg) and bovine serum albumin (BSA), corresponding to masses of 1 ag and 0.11 ag, respectively. To gain the exquisite sensitivity necessary to observe single molecule binding events, a gold nanoshell was used to enhance the optical signal in similar manner as discussed above for single nucleic acid detection (111).

A major challenge in developing protein detection platforms is addressing biological noise. In contrast to nucleic acid analysis that often involves sample isolation or sequence-specific amplification, relevant protein detection applications often involve sensing within complex matrices. These matrices, such as serum, present many off-target protein species that are present at substantially higher concentrations than the target of interest. There have been efforts to minimize off-target binding onto the sensor surface (120, 121), but these approaches have yet to be extended to multiplex sensor operation in clinically relevant samples, such as serum, plasma, and other bodily fluids/tissue homogenates.

Various signal enhancement strategies have been developed to reveal analyte specific sensor responses within complex media. Luchansky et al (122) used sandwich antibody pairs to

enhance signal from protein binding from cellular secretions with limits of detection near 100 pM with an analysis time of only 5 min. Bead-based amplification methods can further extend limits of detection below 100 pg/mL and can be incorporated within an assay scheme giving a total dynamic range of over six orders of magnitude (123, 124). Another method of signal enhancement is the use of enzymatic labels. By attaching an enzyme to tracer antibodies in a sandwich immunoassay, the signal from binding events on the sensor surface can be amplified by rapid turnover of an enzymatic substrate. This method can results in assays with sub-pg/mL detection limits (125). This enzymatic amplification methods was subsequently enabled multiplex phosphoprotein measurements with LODs of 0.6 pM in buffer conditions (Figure 6) (126). The 12-plex phosphoprotein measurements were performed on cell lysate and tumor tissues homogenate of primary glioma samples.

Aside from nucleic acid and protein detection, optical resonator sensors have been applied to other classes of biomolecule detection. Examples of this work include phospholipid modification of microgoblet arrays for investigating lipid binding or other lipid-biomolecule interactions (80, 127). Lipid bilayer assembly dynamics were observed by monitoring bilayer formation in real time (128). This experimental scheme was also used to observe detergent solubilization of lipid bilayers. Microspheres bonded to glass using a modified calcium-assisted glass bonding method have been used to study lipid membrane dynamics with embedded gangliosides (65). For this study, lipid bilayers were transferred onto the sensor substrate using a Langmuir-Blodgett trough.

Beyond in vitro methods for biomolecule detection, free-floating microsphere resonators offer exciting possibilities for in vivo biomolecular imaging. Polystyrene-divinylbenzene (PS-DVB) microspheres can be reproducibly fabricated with radii ranging between 5 and 10 μm, and these microspheres are readily incorporated into eukaryotic cells via endocytosis (85). These particles maintain high Q-factors of up to 10^8 and maintains a 10^4 Q-factor even when engulfed by a single cell (Figure 7). By doping the polymer microspheres with dye, intracellular lasing can be achieved from pumping with 1 nJ pulse energy. Lasing wavelength and pump energy threshold is dependent on microsphere size, refractive index contrast, and dye dopant, and variants in lasing wavelength can be used for specific tagging of individual cells. The narrow spectral linewidth of both the WGM resonance and lasing line provide unambiguous cell barcoding at plexities of 100s to 1000s of unique probes, which is a major improvement over competing labelling methods such as fluorescent dyes and proteins, quantum dots, or plasmonic nanoparticles. Dye-doped microspheres composed of soft materials, such as injected oils or endogenous lipids, can also be used for intracellular lasing (81). Polyphenyl ether (PPE) mixed with Nile red and injected into cells forms small droplets ranging from 4–20 μm in diameter, and lasing occurs upon pulsed excitation with droplets larger than 7 μm. Doped PPE droplets can be used for monitoring the dynamics of cytoplasmic internal stress with sensitivities of 20 pN μm^{-2}. Beyond injected PPE lipids, endogenous lipids present in adipocytes for spherical droplets can support lasing, though at higher excitation energies (Figure 7). Injection of collagenase and a lipophilic dye into the subcutaneous fat layer of porcine tissue releases adipocytes from the tissue matrix, allowing adipocytes to form more spherical shapes. Using an optical fiber inserted through a needle puncture to excite the released adipocytes enabled lasing within tissues (Figure 7).

3.2 Micro-Gas Chromatography

Due to the higher refractive index contrast between sensor and sensing medium, simple sample composition, and improved mass transfer, gas phase sensing is an attractive application for optical resonator sensors, particularly in the realm of gas chromatography. Shopova et al (129) developed the first optical sensor that functioned as a micro gas chromatography detector using a capillary-based optical ring resonator. Here, the microcavity localizes light onto the interior surface of the capillary allowing gas molecules for this detector to be simply flowed as in a standard gas chromatography detection experiment. Scholten et al (76) developed an improved detector from the capillary-based system for microscale gas chromatography by using an optofluidic ring resonator with an optical fiber taper. The system had integrated fluidic connections, and signal response was due to swelling of a 300 nm PDMS layer lining the sensor cavity. The LOD for steady-state sensing was 0.5 ppm for *m*-xylene and ethylbenzene and <10 ppm for all analytes tested. In a follow-up study (78), the authors further developed the microscale gas chromatography system, using a multilayer film composed of polyether doped with gold nanoparticles cast onto the inner wall of the resonator structure to improve the system response. Baseline separation of five volatile organic compounds (VOCs) was achieved in less than 2 min with a detection limit <100 ng. In addition to capillary-and ring-based gas detection systems, porous glass microspheres are also promising for gas detection applications (43).

3.3 Other Sensor Applications

Though the major focus of WGM sensor development in the liquid phase sensing has been on the detection of biomolecules, the sensors are generally applicable to any type of analyte that can be localized to the sensor surface. Panich et al (130) designed a novel sensor for Pb(II) detection in aqueous samples. Glass microsphere resonators coated with aminopropyl trimethoxysilane (APTMS) were subsequently functionalized with glutathione-coated gold nanoparticles. Exposure to Pb(II) resulted in a shift in the resonance peak. The sensor was able to quantitate Pb(II) concentrations ranging from 2 – 50 nM, and operated in the presence of potentially interfering alkaline and heavy metal species. An additional application of interest is the use of microcavity sensors as bulk refractive index detectors for the detection of liquid chromatographic separations. Unlike differential refractometers, microring resonators arrays are compatible with both isocratic and gradient separations methods. Proof-of-concept experiments have been performed on small molecule therapeutics (e.g., ibuprofen) (131). Optical resonators can also been integrated with other analytical tools, such as scanning probe microscopy. Using a 45 μm $BaTiO_3$ microsphere attached to an atomic force microscopy (AFM) cantilever, Wildgen and Dunn (132) performed scanning resonator microscopy. Measurements from this hybrid sensor provide topographical mapping as well as a WGM spectrum that is sensitive to changes in refractive index occurring in the solution as well as on the substrate surface. The method was able to resolve a 36 nm high feature on a glass substrate, and image contrast was derived from refractive index measurements that did not couple with sample tomography. Other proof-of-concept experiments were performed on polymer films and protein-coated surfaces. While not utilized in this study, future applications of scanning resonator microscopy (SRM) could functionalize the surface of the $BaTiO_3$ microsphere with capture agents specific for an analyte of interest on a given substrate, enhancing the utility of the technique.

4. Alternative Sensing Mechanisms

As an alternative to passive microcavities, a new class of active resonator devices that utilize optical gain strategies to achieve detection have recently emerged (133). Much like nanoparticle-induced mode splitting for passive resonators, the splitting of laser emission from active resonators can be used to monitor binding events at the sensor surface, and the pattern of splitting can be detected as a heterodyne beat note, with the beat frequency corresponding to the level of frequency splitting for the lasing modes. Active resonators with low lasing thresholds can be fabricated by doping a SiO_2 microcavity with erbium ($Er:SiO_2$) (134). An Er^{3+} ion dopant concentration of 5×10^8 ions cm^{-3} produces continuous-wave laser operation, enabling several impressive measurements: 30 nm polystyrene and 20 nm gold nanoparticles in air and a single influenza A virus in water. Unfortunately, doping active resonators with rare-earth ions introduces substantial challenges for generating scalable, robust devices due to increased cost of materials and incompatibility with standard CMOS fabrication. Özdemir et al (135) avoided the use of Er^{3+} doping by using Raman gain within a silica microtoroid to create on-chip microlasers. Raman gain is derived from stimulated Raman scattering that occurs with high power pumping, though the necessary input power can be dramatically reduced when coupled with optical microcavities (136). Raman microlasers have the chief benefit of not requiring any dopant for low-threshold lasing, translating into significantly reduced fabrication cost. Using this experimental scheme, nanoparticles as small as 10 nm were detected. Though all experiments were performed in a dry environment, Raman lasers have been demonstrated in liquid environment, making this an intriguing strategy for future sensor development efforts (137).

On-chip lasing and back-scattered light detection can provide substantial reductions in baseline noise, significantly improving LOD over passive optical resonators with wavelength-shift or conventional mode-based sensing mechanisms, but measurement timescales for these devices have been limited to milliseconds or longer. Cavity ring-up spectroscopy (CRUS) can be used with optical resonator sensor to achieve ultrafast sensing, reducing the timescale of measurements to as little as 16 ns (138). The working principle of CRUS derives from the abrupt turn-on of far-detuned probe pulses. The probe pulses are coupled into the optical microcavity with a tapered optical fiber, and since the pulse are detuned away from resonance wavelengths, almost all of the light continues propagating down the optical fiber. The short rise time of the pulse results in large spectral broadening, which overlaps with the resonance conditions and introduces a small field strength in the optical cavity. The electromagnetic field within the resonator constructively interferes with the propagating light creating a ring-up signal. Potential applications of measurements on such precise levels include biological processes such as protein folding or enzyme kinetics (139).

5. Hybrid Sensors

The observation of single binding events with optical resonators was first demonstrated for nanoparticles, using polystyrene beads or viruses as model analytes (33, 86, 91, 92, 134, 140, 141). Novel device designs have recently emerged as method to push the detection limits to the level of single protein and single nucleic acid binding events by incorporating

plasmonic materials with existing WGM sensor designs, which can induce large increases in electric field strength through coupling with localized surface plasmons. This effectively enhances light matter interactions within the evanescent sensing region (142, 143). The most obvious method to combine WGM and plasmonic sensing would be to coat a WGM with a thin layer of noble metals (e.g., Au, Ag); however, large optical losses due to photon scattering substantially reduce the Q-factor for these devices (144). Instead of complete coverage of a sensor surface, single plasmonic nanoparticles bound to the surface of a microcavity sensor allow for signal enhancement by up to 1000-fold while maintaining high Q-factors. These devices have been used for detection of single nanoparticles, viruses, proteins, and nucleic acids. (111, 119, 143, 145). Baaske et al (111) were able to demonstrate discrimination of single base pair mismatches using such approach, as described above and highlighted in Figure 5. A theoretical investigation into WGM-plasmonic hybrid sensors showed that the nanoparticle would exhibit ideal signal enhancement if placed at periodic locations around the equator of a microsphere resonator (145). While this configuration has yet to be experimentally realized, it provides further motivation for the development of this class of hybrid sensing devices.

Optomechanical devices are another type of hybrid sensor that places an optical resonator on a structure that allows for mechanical oscillations via radiation pressure (146). These devices are driven by Brownian fluctuations, which physically displace the resonator, resulting in a change in both the path length and resonant frequency of the microcavity. The sensitivities of these devices are exquisite, approaching the shot noise limit, but device operation in liquid mediums is challenging due to viscous dampening (146). One approach to avoid viscous dampening is to use hollow-core resonator geometries where the solution flows through the center of the structure (147, 148). Fong et al (149) used a suspended microwheel structure embedded in a microfluidic system that allows for stable sensor operation in an aqueous environment. The device is fabricated form 200 nm thick Si_3N_4 with microfluidic channels formed by etching the SiO_2 cladding layer (Figure 8). Light is coupled into the optomechanical resonator via etched gratings and fabricated waveguides. The device impressively allowed for observations of thermal Brownian motion, giving promise for this device in aqueous detection applications. Another demonstration of stable optomechanical operation in liquid environments used GaAs disk resonators placed atop an AlGaAs pedestal (Figure 8) (150). Light coupling was achieved with tapered waveguide structures, and as many as 100 sensors were fabricated on a single 1 mm by 3 mm chip. The devices were stably operated while immersed in water as well as in three perfluorinated liquids with dynamic viscosities measuring 3.5, 9, and 30 mPa s, again allowing observations of thermal Brownian motion.

While not necessarily a hybrid sensor geometry, the Goldsmith group has uniquely utilized microtoroidal resonators in concert with an orthogonal pump bead to perform single particle absorption measurements (151). Silica microtoroids were coated with multi-walled carbon nanotubes. Resonances of the toroid (~1560 nm) were determined via a tapered fiber waveguide while an orthogonal optical pump probe beam at 640 nm was focused and rastered across the surface of the microtoroid. When the probe beam was swept over the nanotube, the absorption and heat dissipation cause shifts in the toroid resonance due to the thermooptic modulation of refractive index. This photothermal microscopy technique hold

promise for the analysis of non-luminescent single particles and molecules. Separately, they showed that in the absence of a chromophore the probe laser itself could be used to heat the silicon pillar, which in turn could be used to tune the resonance wavelength in a controllable fashion (152). However, pillar heating is potentially problematic for single molecule absorption measurements. Accordingly, the same group recently developed a wafer-scale approach to creating silica-, as opposed to silicon, pillared toroidal resonator, and because silica does not absorb light in the visible range, is insensitive to the pump beam (153). While this approach still requires the individual coupling of light into each resonator via a tapered waveguide, the robust process of thermal reflowing, as opposed to laser-based reflowing, seems generally promising for the fabrication of high Q-factor microtoroids.

6. Conclusion

Throughout this review, we have highlighted many examples of applying optical microcavity sensors to a variety of challenging analytical problems. Sensor development has reached the point where fabrication of ultrahigh Q-factor devices capable of detection biomolecules at nanomolar concentrations or below has become routine. Given the breadth of cavity designs and measurement approaches reported to date, it is our opinion that the future of microcavity optical sensors lies in the application and deployment of these devices to real world analytical challenges. Fundamental developments certainly remain to be achieved, but the field is sufficiently mature that these devices should now be expected to emerge as robust tools that can be applied to important chemical and/or biomolecular analysis problems. Given that many of the cavity designs described are realized through microfabrication, one key area for expansion is the creation of multiplexed sensing arrays, which have broad applications ranging from clinical diagnostics to environmental monitoring. The future for microcavity-based devices is bright and their integration within robust analytical instrumentation will facilitate their transition from the optical table and into real-world-deployable systems that will be powerful tools in the ever-evolving analytical arsenal.

References

1. Van Zant, P., Chapman. Microchip Fabrication: A Practical Guide to Semiconductor Processing. McGraw-Hill; New York: 2000.
2. Wiley BJ, Qin D, Xia Y. Nanofabrication at High Throughput and Low Cost. ACS Nano. 2010; 4:3554–9. [PubMed: 20695512]
3. Bogaerts W, Baets R, Dumon P, Wiaux V, Beckx S, et al. Nanophotonic waveguides in silicon-on-insulator fabricated with CMOS technology. J Lightwave Technol. 2005; 23:401–12.
4. Kopp C, Bernabex S, Bakir BB, et al. Silicon Photonic Circuits: On-CMOS Integration, Fiber Optical Coupling, and Packaging. IEEE J Sel Top Quantum Electron. 2011; 17:498–509.
5. Selvaraja SK, Jaenen P, Bogaerts W, Van Thourhout D, Dumon P, Baets R. Fabrication of Photonic Wire and Crystal Circuits in Silicon-on-Insulator Using 193-nm Optical Lithography. J Lightwave Technol. 2009; 27:4076–83.
6. Bogaerts W, Taillaert D, Luyssaert B, Dumon P, Van Campenhout J, et al. Basic structures for photonic integrated circuits in Silicon-on-insulator. Opt Express. 2004; 12:1583–91. [PubMed: 19474984]
7. Orcutt, JS., Khilo, A., Popovic, MA., Holzwarth, CW., Moss, B., et al. Demonstration of an electronic photonic integrated circuit in a commercial scaled bulk CMOS process. Presented at Conference on Lasers and Electro-Optics/Quantum Electronics and Laser Science Conference and Photonic Applications Systems Technologies; 2008.

8. Lipson M. Guiding, modulating, and emitting light on Silicon-challenges and opportunities. J Lightwave Technol. 2005; 23:4222–38.
9. Analui B, Guckenberger D, Kucharski D, Narasimha A. A Fully Integrated 20-Gb/s Optoelectronic Transceiver Implemented in a Standard 0.13-μm CMOS SOI Technology. IEEE J Solid-St Circ. 2006; 41:2945–55.
10. Biberman A, Manipatruni S, Ophir N, Chen L, Lipson M, Bergman K. First demonstration of long-haul transmission using silicon microring modulators. Opt Express. 2010; 18:15544–52. [PubMed: 20720934]
11. Ciminelli C, Campanella CM, Dell'Olio F, Campanella CE, Armenise MN. Label-free optical resonant sensors for biochemical applications. Progress in Quantum Electronics. 2013; 37:51–107.
12. Foreman MR, Swaim JD, Vollmer F. Whispering gallery mode sensors. Adv Opt Photon. 2015; 7:168–240.
13. Vahala KJ. Optical microcavities. Nature. 2003; 424:839–46. [PubMed: 12917698]
14. Wu, Y., Vollmer, F. Cavity-Enhanced Spectroscopy and Sensing. Gagliardi, G., Loock, H-P., editors. Springer; Berlin Heidelberg: 2014. p. 323-49.
15. Rayleigh L. CXII. The problem of the whispering gallery. Philos Mag Series. 1910; 6(20):1001–4.
16. Gorodetsky ML, Savchenkov AA, Ilchenko VS. Ultimate Q of optical microsphere resonators. Opt Lett. 1996; 21:453–5. [PubMed: 19865436]
17. Armani DK, Kippenberg TJ, Spillane SM, Vahala KJ. Ultra-high-Q toroid microcavity on a chip. Nature. 2003; 421:925–8. [PubMed: 12606995]
18. Serpengüzel A, Griffel G, Arnold S. Excitation of resonances of microspheres on an optical fiber. Opt Lett. 1995; 20:654–6. [PubMed: 19859286]
19. Krioukov E, Klunder DJW, Driessen A, Greve J, Otto C. Integrated optical microcavities for enhanced evanescent-wave spectroscopy. Opt Lett. 2002; 27:1504–6. [PubMed: 18026487]
20. Vollmer F, Braun D, Libchaber A, Khoshsima M, Teraoka I, Arnold S. Protein detection by optical shift of a resonant microcavity. Appl Phys Lett. 2002; 80:4057–9.
21. Fan X, White IM. Optofluidic microsystems for chemical and biological analysis. Nat Photon. 2011; 5:591–7.
22. Sun Y, Fan X. Optical ring resonators for biochemical and chemical sensing. Analytical and Bioanalytical Chemistry. 2011; 399:205–11. [PubMed: 20938769]
23. Baaske M, Vollmer F. Optical Resonator Biosensors: Molecular Diagnostic and Nanoparticle Detection on an Integrated Platform. ChemPhysChem. 2012; 13:427–36. [PubMed: 22213654]
24. Bogaerts W, De Heyn P, Van Vaerenbergh T, De Vos K, Kumar Selvaraja S, et al. Silicon microring resonators. Laser Photon Rev. 2012; 6:47–73.
25. Luchansky MS, Bailey RC. High-Q Optical Sensors for Chemical and Biological Analysis. Anal Chem. 2012; 84:793–821. [PubMed: 22111937]
26. Hunt HK, Armani AM. Bioconjugation Strategies for Label-Free Optical Microcavity Sensors. Selected Topics in Quantum Electronics, IEEE Journal of. 2014; 20:121–33.
27. La Notte M, Troia B, Muciaccia T, Campanella C, De Leonardis F, Passaro V. Recent Advances in Gas and Chemical Detection by Vernier Effect-Based Photonic Sensors. Sensors. 2014; 14:4831. [PubMed: 24618728]
28. Mehrabani S, Maker A, Armani A. Hybrid Integrated Label-Free Chemical and Biological Sensors. Sensors. 2014; 14:5890. [PubMed: 24675757]
29. Vivek S, Pao Tai L, Neil P, Hongtao L, Lan L, et al. Mid-infrared materials and devices on a Si platform for optical sensing. Science and Technology of Advanced Materials. 2014; 15:014603. [PubMed: 27877641]
30. Arnold S, Khoshsima M, Teraoka I, Holler S, Vollmer F. Shift of whispering-gallery modes in microspheres by protein adsorption. Opt Lett. 2003; 28:272–4. [PubMed: 12653369]
31. Park Y-S, Wang H. Radiation pressure driven mechanical oscillation in deformed silica microspheres via free-space evanescent excitation. Opt Express. 2007; 15:16471–7. [PubMed: 19550937]
32. Lutti J, Langbein W, Borri P. A monolithic optical sensor based on whispering-gallery modes in polystyrene microspheres. Appl Phys Lett. 2008; 93:151103.

33. Vollmer F, Arnold S, Keng D. Single virus detection from the reactive shift of a whispering-gallery mode. Proc Natl Acad Sci U S A. 2008; 105:20701–4. [PubMed: 19075225]
34. Hossein-Zadeh M, Vahala KJ. Free ultra-high-Q microtoroid: a tool for designing photonic devices. Opt Express. 2007; 15:166–75. [PubMed: 19532232]
35. Kippenberg TJ, Kalkman J, Polman A, Vahala KJ. Demonstration of an erbium-doped microdisk laser on a silicon chip. Phys Rev A. 2006; 74:051802.
36. Lee S, Eom SC, Chang JS, Huh C, Sung GY, Shin JH. A silicon nitride microdisk resonator with 40-nm-thin horizontal air slot. Opt Express. 2010; 18:11209–15. [PubMed: 20588980]
37. Boyd RW, Heebner JE. Sensitive disk resonator photonic biosensor. Appl Opt. 2001; 40:5742–7. [PubMed: 18364865]
38. Chung-Yen C, Fung W, Guo LJ. Polymer microring resonators for biochemical sensing applications. Selected Topics in Quantum Electronics, IEEE Journal of. 2006; 12:134–42.
39. Yalcin A, Popat KC, Aldridge JC, Desai TA, Hryniewicz J, et al. Optical sensing of biomolecules using microring resonators. Selected Topics in Quantum Electronics, IEEE Journal of. 2006; 12:148–55.
40. De Vos K, Bartolozzi I, Schacht E, Bienstman P, Baets R. Silicon-on-Insulator microring resonator for sensitive and label-free biosensing. Opt Express. 2007; 15:7610–5. [PubMed: 19547087]
41. Ling T, Guo LJ. Sensitivity enhancement in optical micro-tube resonator sensors via mode coupling. Applied Physics Letters. 2013; 103:013702.
42. Arce CL, Van Put S, Goes A, Hallynck E, Dubruel P, et al. Reaction tubes: A new platform for silicon nanophotonic ring resonator sensors. Journal of Applied Physics. 2014:115.
43. Wang H, Yuan L, Kim C-W, Lan X, Huang J, et al. Integrated chemical vapor sensor based on thin wall capillary coupled porous glass microsphere optical resonator. Sensors and Actuators B: Chemical. 2015; 216:332–6.
44. Murugan GS, Petrovich MN, Jung Y, Wilkinson JS, Zervas MN. Hollow-bottle optical microresonators. Opt Express. 2011; 19:20773–84. [PubMed: 21997087]
45. McFarlane S, Manchee CPK, Silverstone JW, Veinot J, Meldrum A. Synthesis and Operation of Fluorescent-core Microcavities for Refractometric Sensing. 2013:e50256.
46. Rowland KJ, François A, Hoffmann P, Monro TM. Fluorescent polymer coated capillaries as optofluidic refractometricsensors. Opt Express. 2013; 21:11492–505. [PubMed: 23670006]
47. Lane S, Chan J, Thiessen T, Meldrum A. Whispering gallery mode structure and refractometric sensitivity of fluorescent capillary-type sensors. Sensors and Actuators B: Chemical. 2014; 190:752–9.
48. Ward JM, Dhasmana N, Nic Chormaic S. Hollow core, whispering gallery resonator sensors. Eur Phys J Special Topics. 2014; 223:1917–35.
49. Wang P, Ward J, Yang Y, Feng X, Brambilla G, et al. Lead-silicate glass optical microbubble resonator. Applied Physics Letters. 2015; 106:061101.
50. Gouveia MA, Pellegrini PES, dos Santos JS, Raimundo IM, Cordeiro CMB. Analysis of immersed silica optical microfiber knot resonator and its application as a moisture sensor. Appl Opt. 2014; 53:7454–61. [PubMed: 25402911]
51. Vivien, L., Pavesi, L. Handbook of Silicon Photonics. Taylor & Francis; 2013.
52. Lee H, Chen T, Li J, Yang KY, Jeon S, et al. Chemically etched ultrahigh-Q wedge-resonator on a silicon chip. Nat Photon. 2012; 6:369–73.
53. Kippenberg TJ, Holzwarth R, Diddams SA. Microresonator-Based Optical Frequency Combs. Science. 2011; 332:555–9. [PubMed: 21527707]
54. Wienhold T, Kraemmer S, Wondimu SF, Siegle T, Bog U, et al. All-polymer photonic sensing platform based on whispering-gallery mode microgoblet lasers. Lab Chip. 2015; 15:3800–6. [PubMed: 26266577]
55. Beck, T., Hauser, M., Grossmann, T., Floess, D., Schleede, S., et al. PMMA-micro goblet resonators for biosensing applications. Presented at Proc SPIE 7888, Frontiers in Biological Detection: From Nanosensors to Systems III; 2011.
56. Grossmann T, Hauser M, Beck T, Gohn-Kreuz C, Karl M, et al. High-Q conical polymeric microcavities. Appl Phys Lett. 2010; 96:013303.

57. Qiulin M, Lei H, Zhixiong G, Tobias R. Spectral shift response of optical whispering-gallery modes due to water vapor adsorption and desorption. Meas Sci Technol. 2010; 21:115206.
58. Iqbal M, Gleeson MA, Spaugh B, Tybor F, Gunn WG, et al. Label-Free Biosensor Arrays Based on Silicon Ring Resonators and High-Speed Optical Scanning Instrumentation. IEEE J Sel Top Quantum Electron. 2010; 16:654–61.
59. Wilson KA, Finch CA, Anderson P, Vollmer F, Hickman JJ. Whispering gallery mode biosensor quantification of fibronectin adsorption kinetics onto alkylsilane monolayers and interpretation of resultant cellular response. Biomaterials. 2012; 33:225–36. [PubMed: 21983134]
60. Ramachandran A, Wang S, Clarke J, Ja SJ, Goad D, et al. A universal biosensing platform based on optical micro-ring resonators. Biosens Bioelectron. 2008; 23:939–44. [PubMed: 17964774]
61. Schweinsberg A, Hocdé S, Lepeshkin NN, Boyd RW, Chase C, Fajardo JE. An environmental sensor based on an integrated optical whispering gallery mode disk resonator. Sens Actuat B. 2007; 123:727–32.
62. Masturzo SA, Yarrison-Rice JM, Jackson HE, Boyd JT. Grating Couplers Fabricated by Electron-Beam Lithography for Coupling Free-Space Light Into Nanophotonic Devices. IEEE Trans Nanotechnol. 2007; 6:622–6.
63. Mekis A, Gloeckner S, Masini G, Narasimha A, Pinguet T, et al. A Grating-Coupler-Enabled CMOS Photonics Platform. IEEE J Sel Top Quantum Electron. 2011; 17:597–608.
64. Wildgen S, Dunn R. Whispering Gallery Mode Resonators for Rapid Label-Free Biosensing in Small Volume Droplets. Biosensors. 2015; 5:118. [PubMed: 25806835]
65. Kim DC, Armendariz KP, Dunn RC. Integration of microsphere resonators with bioassay fluidics for whispering gallery mode imaging. Analyst. 2013; 138:3189–95. [PubMed: 23615457]
66. Huckabay HA, Dunn RC. Whispering gallery mode imaging for the multiplexed detection of biomarkers. Sensors and Actuators B: Chemical. 2011; 160:1262–7.
67. Kushida S, Braam D, Pan C, Dao TD, Tabata K, et al. Whispering Gallery Resonance from Self-Assembled Microspheres of Highly Fluorescent Isolated Conjugated Polymers. Macromolecules. 2015; 48:3928–33.
68. Huckabay HA, Wildgen SM, Dunn RC. Label-free detection of ovarian cancer biomarkers using whispering gallery mode imaging. Biosensors and Bioelectronics. 2013; 45:223–9. [PubMed: 23500368]
69. Luchansky MS, Washburn AL, Martin TA, Iqbal M, Gunn LC, Bailey RC. Characterization of the evanescent field profile and bound mass sensitivity of a label-free silicon photonic microring resonator biosensing platform. Biosens Bioelectron. 2010; 26:1283–91. [PubMed: 20708399]
70. Lu X, Lee JY, Feng PX-L, Lin Q. High Q silicon carbide microdisk resonator. Appl Phys Lett. 2014; 104:181103.
71. Cai H, Poon AW. Optical manipulation of microparticles using whispering-gallery modes in a silicon nitride microdisk resonator. Opt Lett. 2011; 36:4257–9. [PubMed: 22048383]
72. Lipka T, Wahn L, Trieu HK, Hilterhaus L, Müller J. Label-free photonic biosensors fabricated with low-loss hydrogenated amorphous silicon resonators. NANOP. 2013; 7:073793.
73. Park J, Ozdemir SK, Monifi F, Chadha T, Huang SH, et al. Titanium Dioxide Whispering Gallery Microcavities. Adv Opt Mat. 2014; 2:711–7.
74. Ioppolo T, gen V, Ayaz U. Development of Whispering Gallery Mode Polymeric Micro-optical Electric Field Sensors. 2013:e50199.
75. Lu Y, Xue Q, Eisele MR, Sulistijo ES, Brower K, et al. Highly multiplexed profiling of single-cell effector functions reveals deep functional heterogeneity in response to pathogenic ligands. Proc Nat Acad Sci. 2015; 112:E607–E15. [PubMed: 25646488]
76. Scholten K, Fan X, Zellers ET. A microfabricated optofluidic ring resonator for sensitive, high-speed detection of volatile organic compounds. Lab Chip. 2014; 14:3873–80. [PubMed: 25131718]
77. De Vos K, Girones J, Claes T, De Koninck Y, Popelka S, et al. Multiplexed Antibody Detection With an Array of Silicon-on-Insulator Microring Resonators. Photonics Journal, IEEE. 2009; 1:225–35.

78. Scholten K, Collin WR, Fan X, Zellers ET. Nanoparticle-coated micro-optofluidic ring resonator as a detector for microscale gas chromatographic vapor analysis. Nanoscale. 2015; 7:9282–9. [PubMed: 25939851]
79. Ta, VD., Chen, R., Sun, H. Flexible microresonators: lasing and sensing. Presented at SPIE LASE; 2014.
80. Bog U, Brinkmann F, Kalt H, Koos C, Mappes T, et al. Large-Scale Parallel Surface Functionalization of Goblet-type Whispering Gallery Mode Microcavity Arrays for Biosensing Applications. Small. 2014; 10:3863–8. [PubMed: 24990526]
81. Humar M, Hyun Yun S. Intracellular microlasers. Nat Photon. 2015 advance online publication.
82. Ta VD, Chen R, Sun HD. Tuning Whispering Gallery Mode Lasing from Self-Assembled Polymer Droplets. Sci Rep. 2013; 4:6396.
83. Delezoide C, Salsac M, Lautru J, Leh H, Nogues C, et al. Vertically Coupled Polymer Microracetrack Resonators for Label-Free Biochemical Sensors. Ieee Photonics Technology Letters. 2012; 24:270–2.
84. Girault P, Lorrain N, Poffo L, Guendouz M, Lemaitre J, et al. Integrated polymer micro-ring resonators for optical sensing applications. Journal of Applied Physics. 2015; 117:104504.
85. Schubert M, Steude A, Liehm P, Kronenberg NM, Karl M, et al. Lasing within Live Cells Containing Intracellular Optical Microresonators for Barcode-Type Cell Tagging and Tracking. Nano Lett. 2015; 15:5647–52. [PubMed: 26186167]
86. Lu T, Lee H, Chen T, Herchak S, Kim J-H, et al. High sensitivity nanoparticle detection using optical microcavities. Proceedings of the National Academy of Sciences. 2011; 108:5976–9.
87. Xu DX, Vachon M, Densmore A, Ma R, Janz S, et al. Real-time cancellation of temperature induced resonance shifts in SOI wire waveguide ring resonator label-free biosensor arrays. Opt Express. 2010; 18:22867–79. [PubMed: 21164626]
88. Shao L, Jiang X-F, Yu X-C, Li B-B, Clements WR, et al. Detection of Single Nanoparticles and Lentiviruses Using Microcavity Resonance Broadening. Advanced Materials. 2013; 25:5616–20. [PubMed: 24303524]
89. Foreman MR, Jin W-L, Vollmer F. Optimizing detection limits in whispering gallery mode biosensing. Opt Express. 2014; 22:5491–511. [PubMed: 24663890]
90. Kim W, Özdemir ŞK, Zhu J, Yang L. Observation and characterization of mode splitting in microsphere resonators in aquatic environment. Applied Physics Letters. 2011; 98:141106.
91. Zhu J, Özdemir ŞK, He L, Chen D-R, Yang L. Single virus and nanoparticle size spectrometry by whispering-gallery-mode microcavities. Opt Express. 2011; 19:16195–206. [PubMed: 21934982]
92. Zhu J, Ozdemir SK, Xiao Y-F, Li L, He L, et al. On-chip single nanoparticle detection and sizing by mode splitting in an ultrahigh-Q microresonator. Nature Photonics. 2010; 4:46–9.
93. Knittel J, Swaim JD, McAuslan DL, Brawley GA, Bowen WP. Back-scatter based whispering gallery mode sensing. Sci Rep. 2013; 3:2974. [PubMed: 24131939]
94. Noto M, Keng D, Teraoka I, Arnold S. Detection of Protein Orientation on the Silica Microsphere Surface Using Transverse Electric/Transverse Magnetic Whispering Gallery Modes. Biophys J. 92:4466–72.
95. Zamora V, Lützow P, Weiland M, Pergande D. A Highly Sensitive Refractometric Sensor Based on Cascaded SiN Microring Resonators. Sensors. 2013; 13:14601. [PubMed: 24169543]
96. Sedlmeir F, Zeltner R, Leuchs G, Schwefel HGL. High-Q MgF2 whispering gallery mode resonators for refractometric sensing in aqueous environment. Opt Express. 2014; 22:30934–42. [PubMed: 25607042]
97. Hermanson, GT. Bioconjugate techniques. Academic press; 2013.
98. Green N. Avidin. 1. The use of [14C] biotin for kinetic studies and for assay. Biochem J. 1963; 89:585. [PubMed: 14101979]
99. Suter JD, White IM, Zhu H, Shi H, Caldwell CW, Fan X. Label-free quantitative DNA detection using the liquid core optical ring resonator. Biosens Bioelectron. 2008; 23:1003–9. [PubMed: 18036809]

100. Vollmer F, Arnold S, Braun D, Teraoka I, Libchaber A. Multiplexed DNA Quantification by Spectroscopic Shift of Two Microsphere Cavities. Biophys J. 2003; 85:1974–9. [PubMed: 12944310]
101. Qavi AJ, Mysz TM, Bailey RC. Isothermal Discrimination of Single-Nucleotide Polymorphisms via Real-Time Kinetic Desorption and Label-Free Detection of DNA Using Silicon Photonic Microring Resonator Arrays. Anal Chem. 2011; 83:6827–33. [PubMed: 21834517]
102. Shin Y, Perera AP, Park MK. Label-free DNA sensor for detection of bladder cancer biomarkers in urine. Sensors and Actuators B: Chemical. 2013; 178:200–6.
103. Sabaté del Río J, Steylaerts T, Henry OYF, Bienstman P, Stakenborg T, et al. Real-time and label-free ring-resonator monitoring of solid-phase recombinase polymerase amplification. Biosensors and Bioelectronics. 2015; 73:130–7. [PubMed: 26056956]
104. Wu Y, Zhang DY, Yin P, Vollmer F. Ultraspecific and Highly Sensitive Nucleic Acid Detection by Integrating a DNA Catalytic Network with a Label-Free Microcavity. Small. 2014; 10:2067–76. [PubMed: 24585636]
105. Egger G, Liang G, Aparicio A, Jones PA. Epigenetics in human disease and prospects for epigenetic therapy. Nature. 2004; 429:457–63. [PubMed: 15164071]
106. Hawk RM, Armani AM. Label free detection of 5′hydroxymethylcytosine within CpG islands using optical sensors. Biosensors and Bioelectronics. 2015; 65:198–203. [PubMed: 25461158]
107. Shin Y, Soo RA, Yoon J, Promoda Perera A, Yoon Y-J, Park MK. Rapid and label-free amplification and detection assay for genotyping of cancer biomarker. Biosensors and Bioelectronics. 2015; 68:107–14. [PubMed: 25569872]
108. Kindt JT, Bailey RC. Chaperone Probes and Bead-Based Enhancement To Improve the Direct Detection of mRNA Using Silicon Photonic Sensor Arrays. Anal Chem. 2012; 84:8067–74. [PubMed: 22913333]
109. Chomczynski P, Sacchi N. Single-step method of RNA isolation by acid guanidinium thiocyanate-phenol-chloroform extraction. Anal Biochem. 1987; 162:156–9. [PubMed: 2440339]
110. Blin N, Stafford DW. A general method for isolation of high molecular weight DNA from eukaryotes. Nucleic Acids Res. 1976; 3:2303–8. [PubMed: 987581]
111. Baaske MD, Foreman MR, Vollmer F. Single-molecule nucleic acid interactions monitored on a label-free microcavity biosensor platform. Nat Nano. 2014; 9:933–9.
112. Bayley H, Cremer PS. Stochastic sensors inspired by biology. Nature. 2001; 413:226–30. [PubMed: 11557992]
113. Shia WW, Bailey RC. Single Domain Antibodies for the Detection of Ricin Using Silicon Photonic Microring Resonator Arrays. Anal Chem. 2013; 85:805–10. [PubMed: 23268548]
114. Nunzi Conti G, Baldini F, Berneschi S, Farnesi D, Giannetti A, et al. Whispering gallery mode microresonators: results on aptasensors and on a new sensing approach. 2013
115. Park MK, Kee JS, Quah JY, Netto V, Song J, et al. Label-free aptamer sensor based on silicon microring resonators. Sensors and Actuators B: Chemical. 2013; 176:552–9.
116. Chibli H, Ghali H, Park S, Peter Y-A, Nadeau JL. Immobilized phage proteins for specific detection of staphylococci. Analyst. 2014; 139:179–86. [PubMed: 24255915]
117. Fan XZ, Naves L, Siwak NP, Brown A, Culver J, Ghodssi R. Integration of genetically modified virus-like-particles with an optical resonator for selective bio-detection. Nanotechnology. 2015; 26:205501. [PubMed: 25915182]
118. Shia WW, Bailey RC. Single Domain Antibodies for the Detection of Ricin Using Silicon Photonic Microring Resonator Arrays. Analytical Chemistry. 2012; 85:805–10. [PubMed: 23268548]
119. Dantham VR, Holler S, Barbre C, Keng D, Kolchenko V, Arnold S. Label-Free Detection of Single Protein Using a Nanoplasmonic-Photonic Hybrid Microcavity. Nano Letters. 2013; 13:3347–51. [PubMed: 23777440]
120. Lin S, Diercks CS, Zhang Y-B, Kornienko N, Nichols EM, et al. Covalent organic frameworks comprising cobalt porphyrins for catalytic CO2 reduction in water. Science. 2015
121. Wang F, Anderson M, Bernards M, Hunt H. PEG Functionalization of Whispering Gallery Mode Optical Microresonator Biosensors to Minimize Non-Specific Adsorption during Targeted, Label-Free Sensing. Sensors. 2015; 15:18040. [PubMed: 26213937]

122. Luchansky MS, Bailey RC. Rapid, Multiparameter Profiling of Cellular Secretion Using Silicon Photonic Microring Resonator Arrays. J Am Chem Soc. 2011; 133:20500–6. [PubMed: 22040005]

123. Valera E, McClellan MS, Bailey RC. Magnetically-actuated, bead-enhanced silicon photonic immunosensor. Anal Methods. 2015; 7:8539–44. [PubMed: 26528374]

124. Luchansky MS, Washburn AL, McClellan MS, Bailey RC. Sensitive on-chip detection of a protein biomarker in human serum and plasma over an extended dynamic range using silicon photonic microring resonators and sub-micron beads. Lab Chip. 2011; 11:2042–4. [PubMed: 21541438]

125. Kindt JT, Luchansky MS, Qavi AJ, Lee S-H, Bailey RC. Subpicogram Per Milliliter Detection of Interleukins Using Silicon Photonic Microring Resonators and an Enzymatic Signal Enhancement Strategy. Analytical Chemistry. 2013; 85:10653–7. [PubMed: 24171505]

126. Wade JH, Alsop AT, Vertin NR, Yang H, Johnson MD, Bailey RC. Rapid, Multiplexed Phosphoprotein Profiling Using Silicon Photonic Sensor Arrays. ACS Cent Sci. 2015; 1:374–82. [PubMed: 26539563]

127. Bog U, Laue T, Grossmann T, Beck T, Wienhold T, et al. On-chip microlasers for biomolecular detection via highly localized deposition of a multifunctional phospholipid ink. Lab Chip. 2013; 13:2701–7. [PubMed: 23649356]

128. Sun V, Armani AM. Real-time detection of lipid bilayer assembly and detergent-initiated solubilization using optical cavities. Applied Physics Letters. 2015; 106:071103. [PubMed: 25759510]

129. Shopova SI, White IM, Sun Y, Zhu H, Fan X, et al. On-Column Micro Gas Chromatography Detection with Capillary-Based Optical Ring Resonators. Anal Chem. 2008; 80:2232–8. [PubMed: 18271605]

130. Panich S, Wilson KA, Nuttall P, Wood CK, Albrecht T, Edel JB. Label-Free Pb(II) Whispering Gallery Mode Sensing Using Self-Assembled Glutathione-Modified Gold Nanoparticles on an Optical Microcavity. Analytical Chemistry. 2014; 86:6299–306. [PubMed: 24871358]

131. Wade JH, Bailey RC. Refractive Index-Based Detection of Gradient Elution Liquid Chromatography using Chip-Integrated Microring Resonator Arrays. Analytical Chemistry. 2014; 86:913–9. [PubMed: 24328221]

132. Wildgen SM, Dunn RC. Scanning Resonator Microscopy: Integrating Whispering Gallery Mode Sensing with Atomic Force Microscopy. ACS Photonics. 2015; 2:699–706.

133. Ernst GJ, Witteman WJ. Mode structure of active resonators. IEEE J Quantum Electron. 1973; 9:911–8.

134. He L, Oezdemir SK, Zhu J, Kim W, Yang L. Detecting single viruses and nanoparticles using whispering gallery microlasers. Nature Nanotechnology. 2011; 6:428–32.

135. Özdemir ŞK, Zhu J, Yang X, Peng B, Yilmaz H, et al. Highly sensitive detection of nanoparticles with a self-referenced and self-heterodyned whispering-gallery Raman microlaser. Proceedings of the National Academy of Sciences. 2014; 111:E3836–E44.

136. Grudinin IS, Maleki L. Ultralow-threshold Raman lasing with CaF2 resonators. Opt Lett. 2007; 32:166–8. [PubMed: 17186052]

137. Chistiakova MV, Armani AM. Cascaded Raman microlaser in air and buffer. Opt Lett. 2012; 37:4068–70. [PubMed: 23027281]

138. Rosenblum S, Lovsky Y, Arazi L, Vollmer F, Dayan B. Cavity ring-up spectroscopy for ultrafast sensing with optical microresonators. Nat Commun. 2015:6.

139. Mayor U, Guydosh NR, Johnson CM, Grossmann JG, Sato S, et al. The complete folding pathway of a protein from nanoseconds to microseconds. Nature. 2003; 421:863–7. [PubMed: 12594518]

140. Arnold S, Keng D, Shopova SI, Holler S, Zurawsky W, Vollmer F. Whispering gallery mode carousel – a photonic mechanism for enhanced nanoparticle detection in biosensing. Opt Express. 2009; 17:6230–8. [PubMed: 19365447]

141. Lin S, Crozier KB. Planar silicon microrings as wavelength-multiplexed optical traps for storing and sensing particles. Lab Chip. 2011; 11:4047–51. [PubMed: 22011760]

142. Santiago-Cordoba MA, Cetinkaya M, Boriskina SV, Vollmer F, Demirel MC. Ultrasensitive detection of a protein by optical trapping in a photonic-plasmonic microcavity. Journal of Biophotonics. 2012; 5:629–38. [PubMed: 22707455]

143. Shopova SI, Rajmangal R, Holler S, Arnold S. Plasmonic enhancement of a whispering-gallery-mode biosensor for single nanoparticle detection. Applied Physics Letters. 2011; 98:243104.

144. Min B, Ostby E, Sorger V, Ulin-Avila E, Yang L, et al. High-Q surface-plasmon-polariton whispering-gallery microcavity. Nature. 2009; 457:455–U3. [PubMed: 19158793]

145. Arnold S, Dantham VR, Barbre C, Garetz BA, Fan X. Periodic plasmonic enhancing epitopes on a whispering gallery mode biosensor. Opt Express. 2012; 20:26147–59. [PubMed: 23187470]

146. Kippenberg TJ, Vahala KJ. Cavity opto-mechanics. Opt Express. 2007; 15:17172–205. [PubMed: 19551012]

147. Burg TP, Godin M, Knudsen SM, Shen W, Carlson G, et al. Weighing of biomolecules, single cells and single nanoparticles in fluid. Nature. 2007; 446:1066–9. [PubMed: 17460669]

148. Kim KH, Bahl G, Lee W, Liu J, Tomes M, et al. Cavity optomechanics on a microfluidic resonator with water and viscous liquids. Light-Science & Applications. 2013:2.

149. Fong KY, Poot M, Tang HX. Nano-Optomechanical Resonators in Microfluidics. Nano Lett. 2015; 15:6116–20. [PubMed: 26226184]

150. Gil-Santos E, Baker C, Nguyen DT, Hease W, Gomez C, et al. High-frequency nano-optomechanical disk resonators in liquids. Nat Nanotechnol. 2015; 10:810–6. [PubMed: 26237347]

151. Heylman KD, Knapper KA, Goldsmith RH. Photothermal Microscopy of Nonluminescent Single Particles Enabled by Optical Microresonators. J Phys Chem Lett. 2014; 5:1917–23. [PubMed: 26273873]

152. Heylman KD, Goldsmith RH. Photothermal mapping and free-space laser tuning of toroidal optical microcavities. Appl Phys Lett. 2013; 103:211116.

153. Knapper K, Goldsmith R. 2016 In Press.

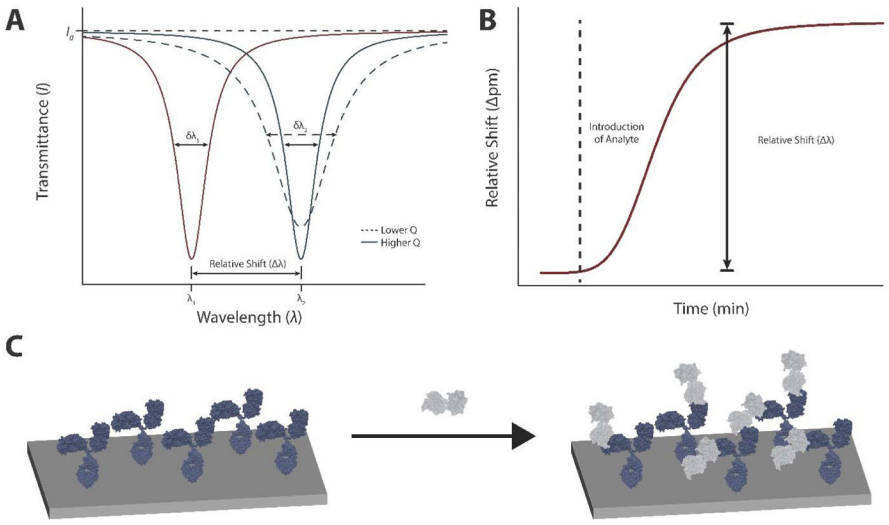

Figure 1. Overview of Sensor Operation

(**A**) The transmission spectrum from a tunable laser interfaced with a whispering gallery mode resonator results in characteristic dip in transmittance under resonance conditions. Changes to the local refractive index at the sensor surface cause a shift in the resonance wavelength (solid red vs solid blue traces). In addition to wavelength shifts, changes in the quality (Q) factor can occur, with a lower Q-factor resulting in a broadening of spectral linewidth ($\delta\lambda$, dashed blue trace). (**B**) Plotting relative wavelength shifts versus time produces a characteristic Langmuir binding curve. (**C**) One example of optical resonators as sensors is in protein detection, and the schematic shows a protein (white) binding to antibodies (blue) bound to a sensor surface.

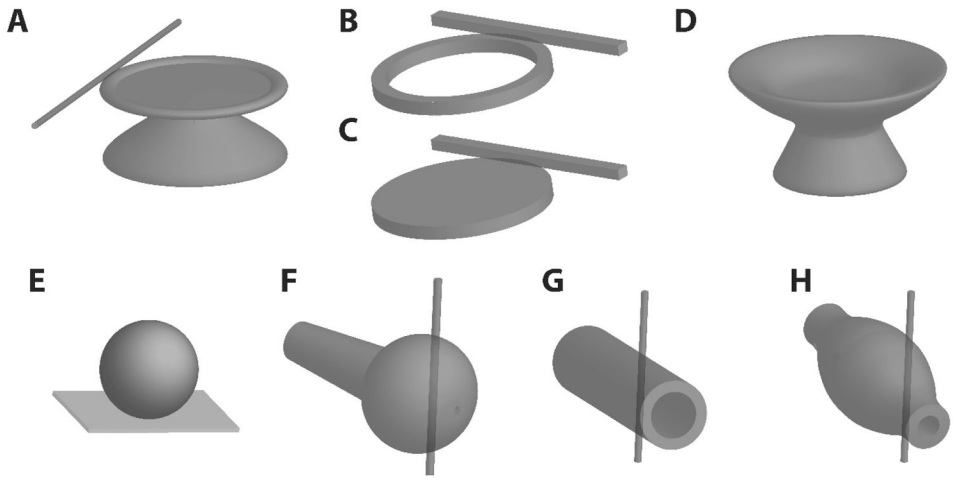

Figure 2. Microcavity Resonator Sensor Geometries

Many circular geometries have been used for fabrication of whispering gallery mode sensors. Some of the more common designs include microtoroids (**A**), microrings (**B**), microdisks (**C**), microgoblets (**D**), microspheres fabricated with (**F**) or without (**E**) attached optical fibers, microcapillaries (**G**), and microbubbles (**H**).

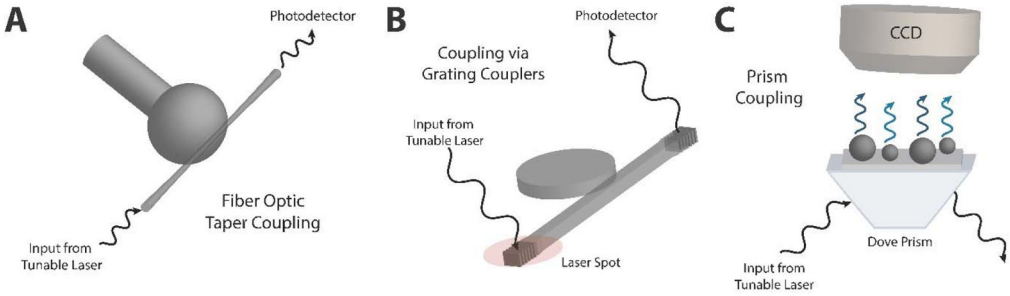

Figure 3. Sensing Mechanisms for Optical Microcavity Resonators

(**A**) Fiber optic taper coupling requires the precise alignment of an optical fiber with microcavity sensor. Output can be monitored with a photodetector, measuring current over time. Though the alignment can be arduous, this method allows for highly efficient coupling [e.g., Refs (106, 120)]. (**B**) Grating couplers allow for on-chip coupling without the demands of precise fiber alignment, though at the cost of lower coupling efficiencies. Output is very similar to fiber optic coupling [e.g., Ref (58)]. (**C**) Prism coupling can be used in cases where sensors (e.g., microspheres) are attached directly to a surface. The presented example shows fluorescent microspheres that can be used for whispering gallery mode imaging [e.g., Refs (65, 68).]

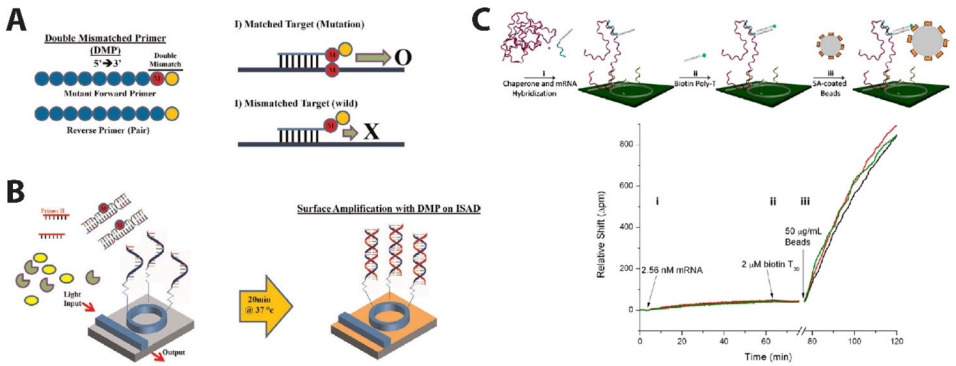

Figure 4. Amplification of Nucleic Acids for Detection in Complex Media

(**A**) A schematic of the double mismatch primer (DMP) method is shown for detection of mutant sequences with a background of wild type DNA strands. Amplification occurs with greatest efficiency when the mismatched forward mutant primer binds to the matched mutant target [Ref (107)]. (**B**) Amplification is performed on DMP modified sensor chips with the addition of recombinase (yellow) and polymerase (green), and detection was achieved in spiked urine samples. (**C**) An assay schematic shows the sequential steps necessary for mRNA detection: (i) hybridization of chaperone DNA molecules with target mRNA, (ii) binding of biotinylated linker strands and blocking of the sensor surface, and (iii) introduction of streptavidin coated beads to bind to biotinylated linker strands. The representative spectrum (bottom) shows real time monitoring of binding events with a sharp increase in sensor response upon the introduction of beads. mRNA transcripts detected using this method were derived from RNA extracts from HL-60 cells [Ref (108)].

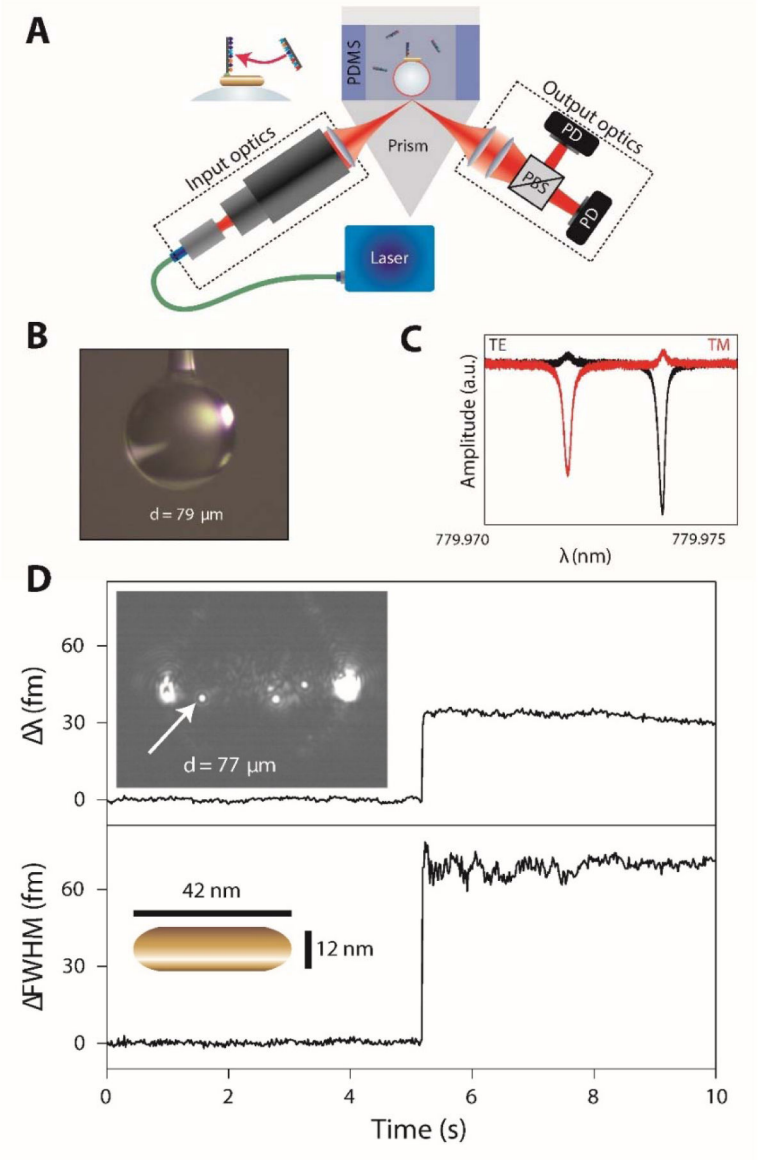

Figure 5. Ultrasensitive Detection of Nucleic Acids

(**A**) The assay schematic shows incorporation light into the microsphere cavity via prism coupling and a single nanorod attached to the sensor surface. A PDMS microchamber was used as a flow cell for analyte introduction. (**B**) Image of a microsphere fabricated by melting the tip of an optical fiber. (**C**) An example transmission spectrum for the microsphere (without a nanorod attached) showing both transverse electric (TE) and transverse magnetic (TM) propagating modes. (**D**) The adsorption of cetyltrimethylammonium bromide (CTAB) stabilized nanorods occurs at a pH of 1.6. Top is the relative shift for the TM mode, and bottom is the change is a measurement of band broadening ($\delta\lambda$). The top inset shows an optical micrograph of an excited microsphere with a single nanorod (identified with the arrow) adsorbed to the microsphere surface with the nanorod dimensions shown in the bottom inset. Adapted from ref (111).

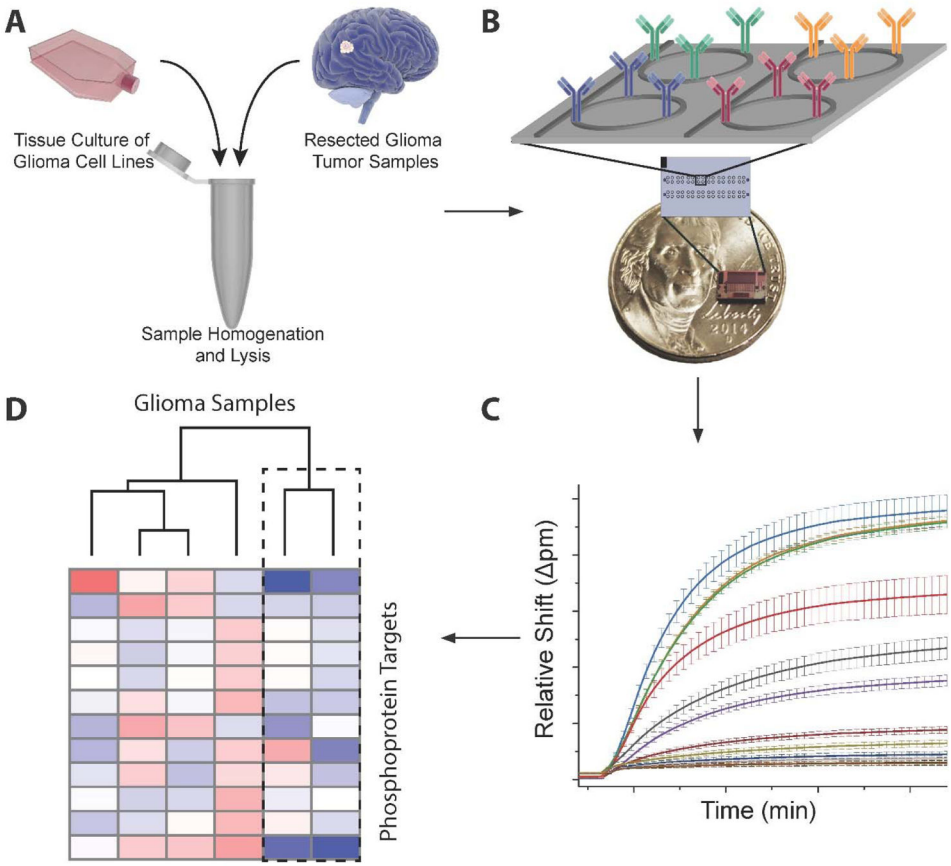

Figure 6. Multiplex Phosphoprotein Detection in Cell Lysate and Tumor Tissue Homogenate

(**A**) Samples form primary surgical glioma samples or tissue culture were homogenized and lysed. (**B**) Cell lysate was flowed across a microring resonator array modified with antibodies specific for phosphoprotein targets. (**C**) Sample output from a single chip is shown with signal enhancement achieved using a sandwich immunoassay with enzymatic amplification. (**D**) Phosphoprotein expression profiling with the microring resonator platform was used to analyze primary surgical glioma specimens. Sorting with unsupervised hierarchical clustering separated two samples, and these specimens contained >50% necrotic tissues, as determined from pathology reports. Adapted from Ref..

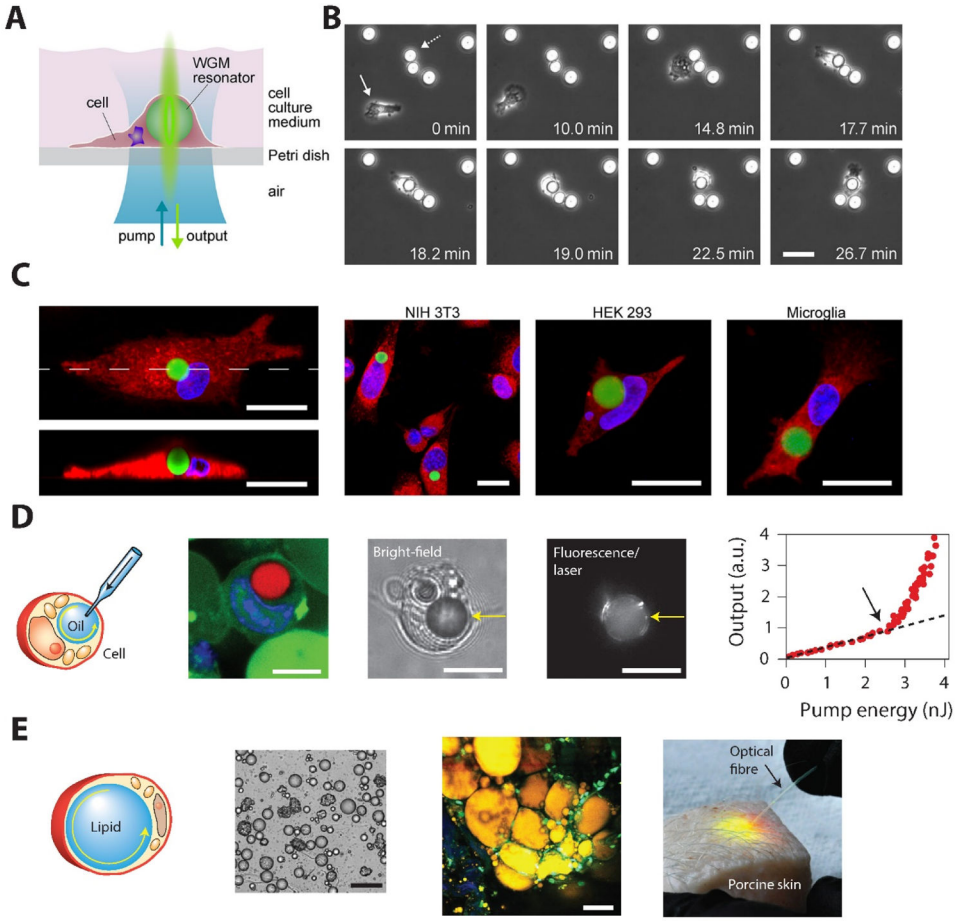

Figure 7. Intracellular Lasing with Polymer Microspheres and Oil Droplets

(**A**) A schematic of the intracellular laser with optical pumping and detection achieved through a common optical path from beneath the cell culture dish. (**B**) Time-lapse microscopy of polymer microspheres added to macrophage culture shows internalization of the microspheres. (**C**) Confocal microscopy of stained macrophages and microsphere resonators demonstrate that the microspheres are internalized in a variety of lines (85). Soft materials such as oil droplets (**D**) and endogenous lipid droplets (**E**) can also be used for intracellular lasing. (**D**) From left to right, lasing with injected oil droplets is shown with a schematic or oil injection, confocal fluorescence of a cell with an injected oil droplet (blue = nucleus, red = oil droplet), bright field and laser output from an oil droplet with optical pumping, and a plot of optical output as a function of pump energy. (**E**) Intracellular lasing can be similarly achieved with endogenous lipids as is shown (from left to right) by the illustration of a subcutaneous adipocyte, optical micrograph of adipocytes from porcine fat, two-photon confocal imaging of subcutaneous fat tissue after injection of a dye (yellow), and image of intracellular lasing within porcine tissue (81).

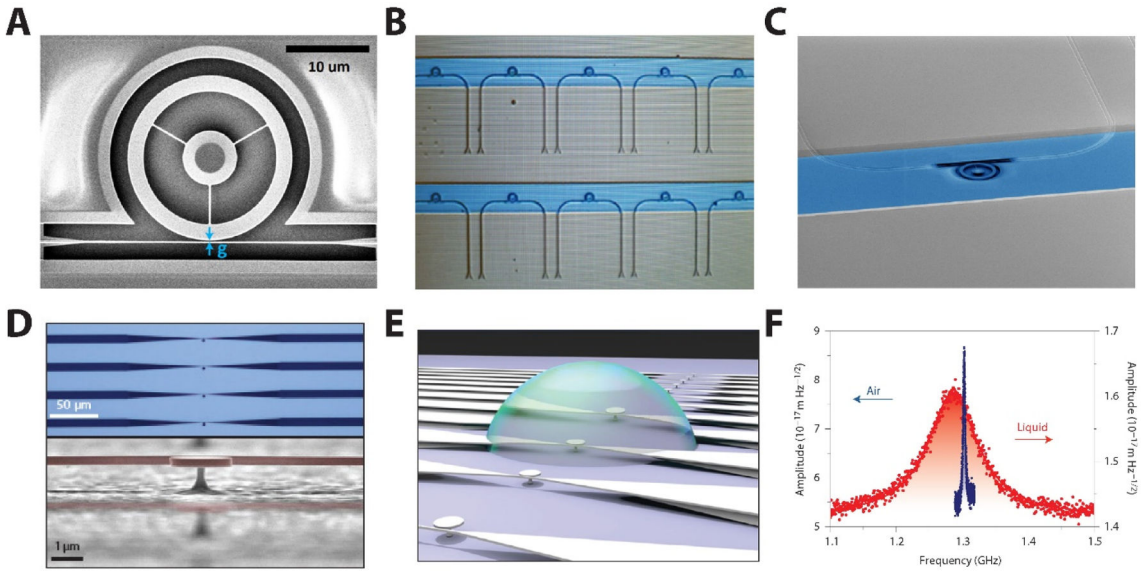

Figure 8. Hybrid Optomechanical Sensors

(**A**) A scanning electron micrograph (SEM) of optomechanical microwheel resonator with an adjacent coupling waveguide shows the top view of the device. (**B**) An optical image demonstrates an array of microwheel resonators embedded in microfluidic channels (blue). (**C**) An angled view SEM shows the device structure positioned within the microfluidic channel (blue). (**D**) Top: Optical image of four disk resonators with adjacent tapered waveguides. Bottom: An angled view SEM of GaAs disk (red) resonators atop AlGaAs pedestal. The tapered optical waveguide (red) is behind the GaAs disk (also red). (**E**) A schematic depicts immersing the resonators in a liquid droplet. (**F**) Thermomechanical spectra acquired from optomechanical measurements demonstrates resonator motion before (blue) and after (red) immersion in liquid.